Supplemental Materials:

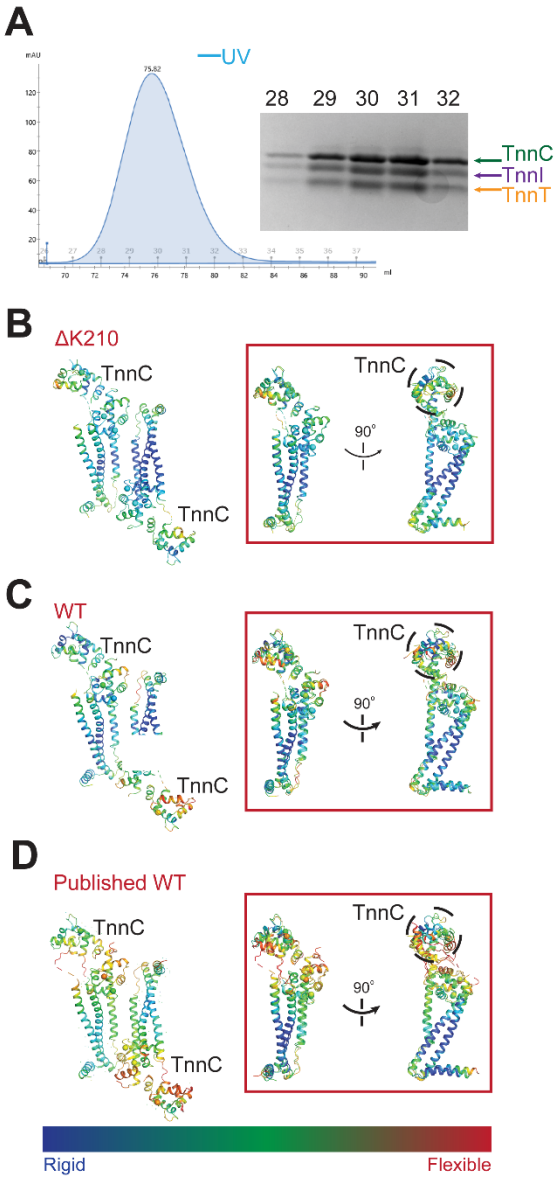

Figure S1. Structure comparison of WT and ΔK210 complex. (A) Size-exclusion chromatography (Superdex 200) of the WT complex. The Y axis shows the absorbance at 280 nm and the X axis shows the elution volume in ml. Peak fractions were analyzed by SDS-PAGE and visualized with Stain-Free dye (Biorad). **(B)** Left: Cartoon representation of the overall structure of ΔK210 complex colored by b factor. Right in the red box: Cartoon representation showing superimposition of two protomers in the asymmetric unit of ΔK210 complex colored by b factor. **(C)** Left: Cartoon representation of the overall structure of WT complex colored by b factor. Right in the red box: Cartoon representation showing superimposition of two protomers in the asymmetric unit of WT complex colored by b factor. **(D)** Left: Cartoon representation of the overall structure of published

WT. complex (PDB: 1J1D) colored by b factor. Right in the red box: Cartoon representation showing superimposition of two protomers in the asymmetric unit of published WT complex colored by b factor.

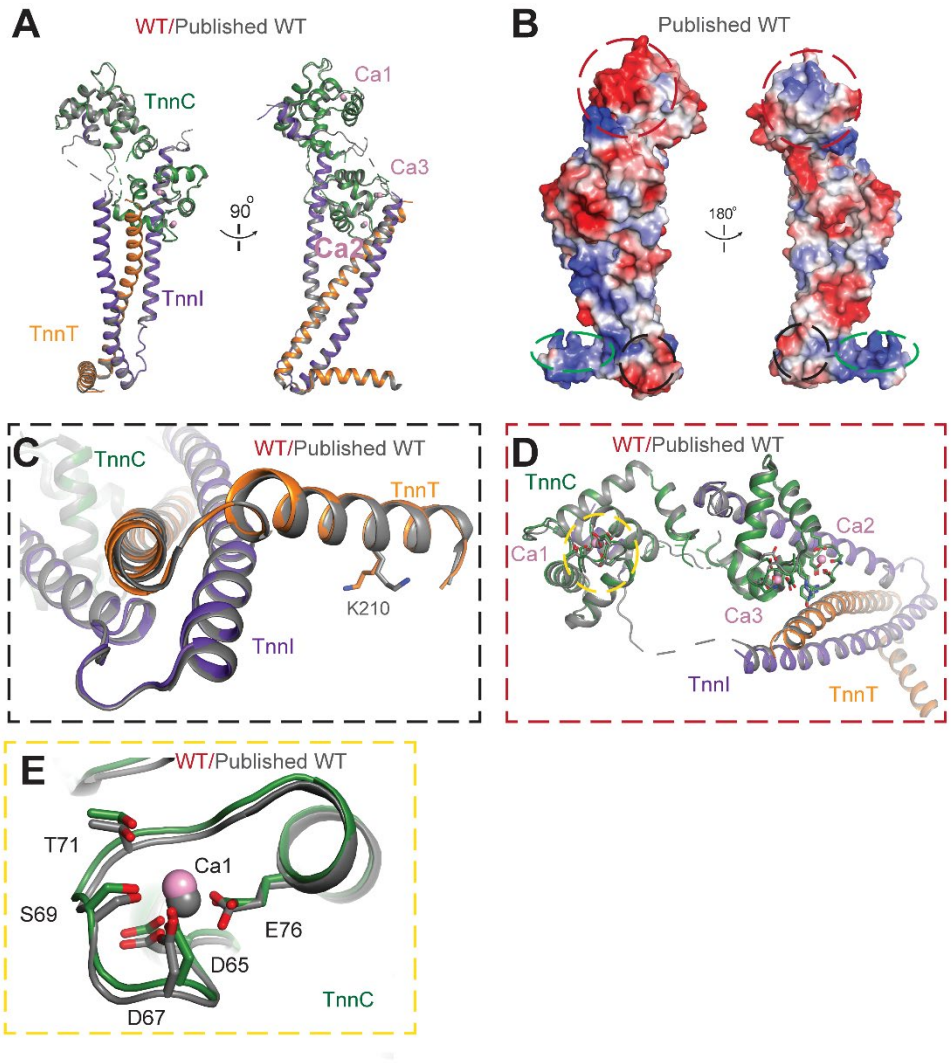

Figure S2. Structure highlight of K210 in WT and ΔK210 complex. (A) Cartoon representation showing superimposition of WT (TnnC in green, TnnT in orange and TnnI in purple) and published WT complex (PDB: 1J1D). **(B)** Surface representation colored by the vacuum electrostatic potential of the published WT complex. **(C)** Highlight of K210 site and hinge region of TnnT and TnnI showing superimposition of WT (TnnC in green, TnnT in orange and TnnI in purple) and published WT (grey). **(D)** Cartoon representation showing superimposition of TnnC in WT and published WT (grey). **(E)** Cartoon representation showing superimposition of the detailed interaction of Ca^{2+} in the activation Ca^{2+} binding pocket for TnnC in WT (green) and published WT (grey).

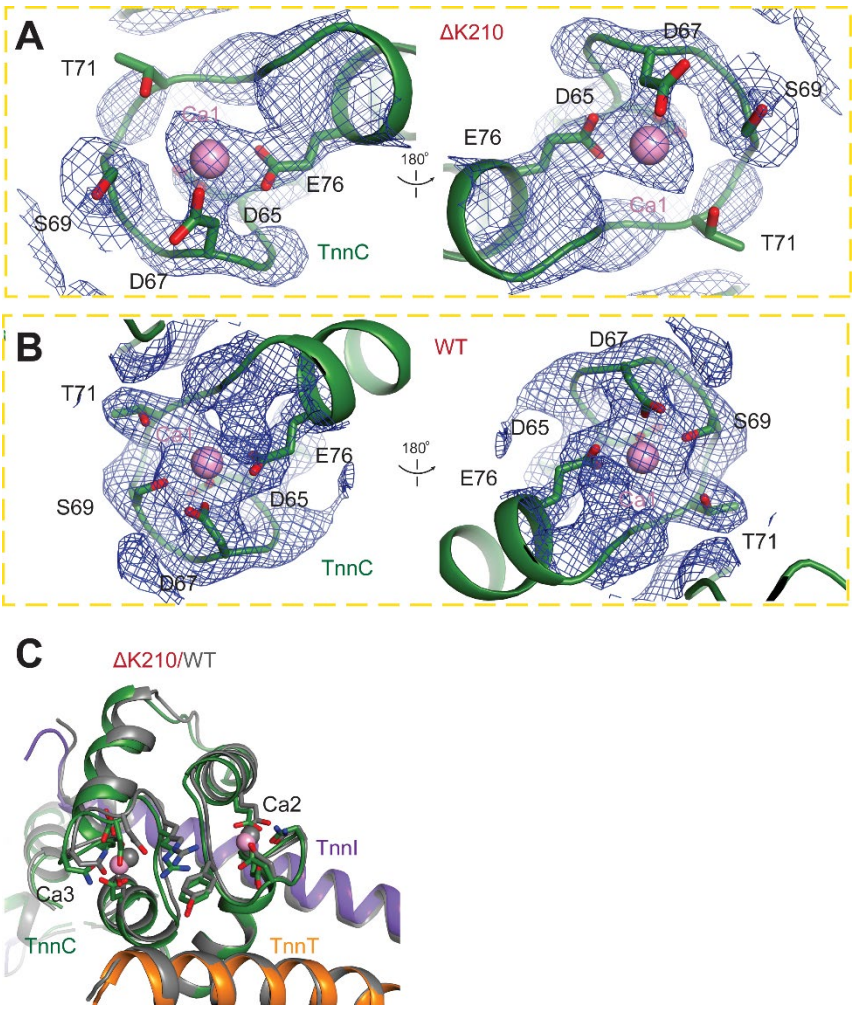

Figure S3. Structure details of Ca^{2+} binding site in WT and ΔK210 complex. (A) Simulated annealing omit map of Ca^{2+} coordination in the activation Ca^{2+} binding pocket for TnnC in ΔK210 complex. TnnC is shown in green, TnnT is shown in orange and TnnI is shown in purple. Ca^{2+} is shown in pink sphere. **(B)** Simulated annealing omit map of Ca^{2+} coordination in the activation Ca^{2+} binding pocket for TnnC in WT complex. **(C)** Cartoon representation showing superimposition of the structural Ca^{2+}binding domain of TnnC in WT (grey) and ΔK210 (TnnC in green, TnnT in orange and TnnI in purple).

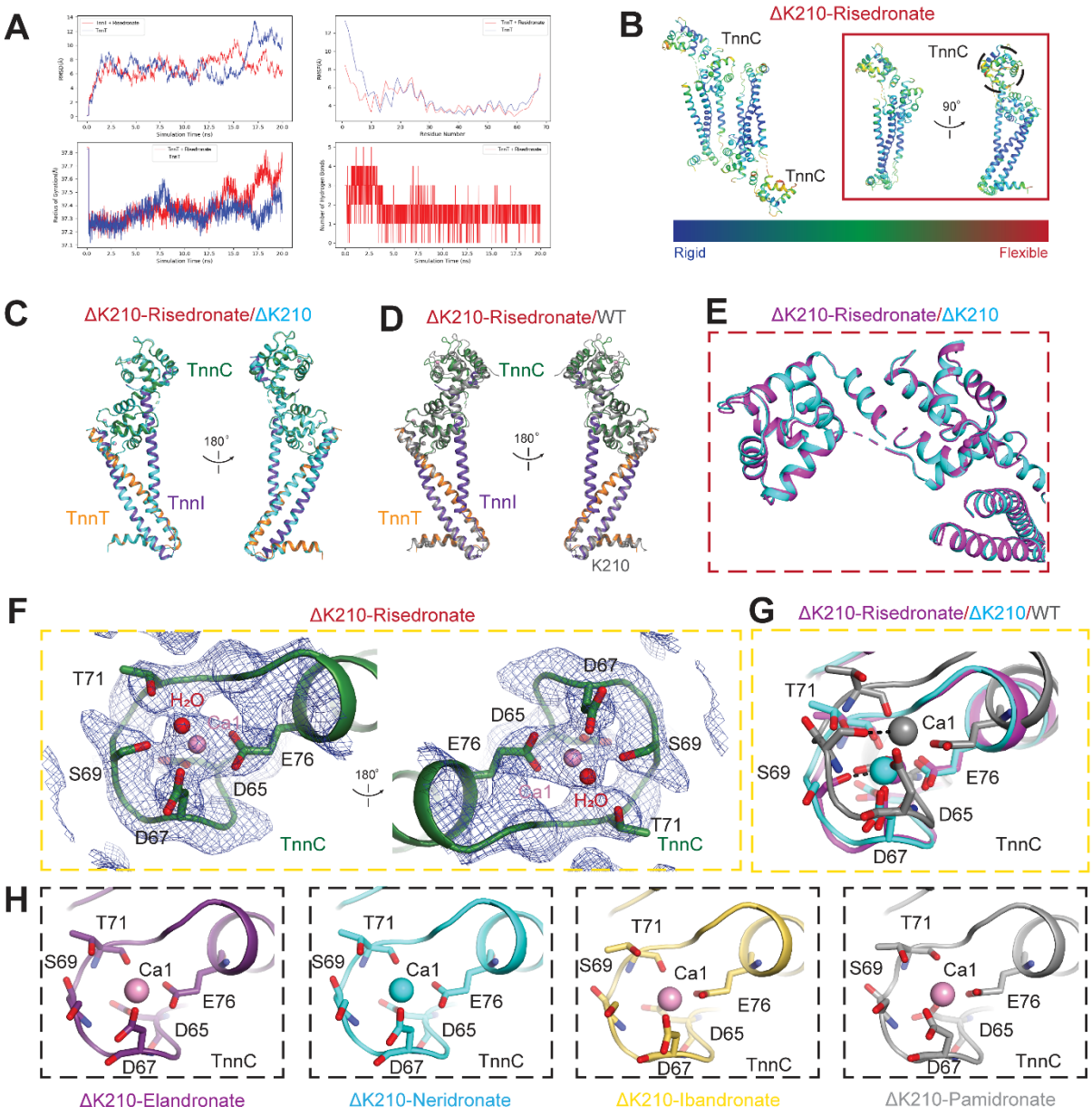

Figure S4. Structure simulation of WT and ΔK210 complex at the presence of risedronate. (A) RMSD, RMSF, Radius of gyration, and number of hydrogen bonds are the main parameters for molecular dynamic simulations over 20 ns for mutated (K210del) alone and with risedronate. **(B)** Left: Cartoon representation of the overall structure of ΔK210 complex in the presence of risedronate acid colored by b factor. Right in the red box: Cartoon representation showing superimposition of two protomers in the asymmetric unit of ΔK210 complex in the presence of risedronate acid colored by b factor. **(C)** Cartoon representation showing superimposition of ΔK210 complex (cyan) and ΔK210 complex in the presence of risedronate (TnnC in green, TnnT in orange and TnnI in purple). **(D)** Cartoon representation showing superimposition of WT complex (grey) and ΔK210 complex in

the presence of risedronate (TnnC in green, TnnT in orange and TnnI in purple). **(E)** Cartoon representation showing superimposition of TnnC in ΔK210 complex in the presence of risedronate (purple) and ΔK210 complex (cyan). **(F)** Simulated annealing omit map of Ca^{2+} coordination in the activation Ca^{2+} binding pocket for TnnC in ΔK210 complex in the presence of risedronate. TnnC is shown in green, TnnT is shown in orange and TnnI is shown in purple. Ca^{2+} is shown in pink sphere. **(G)** Cartoon representation showing superimposition of the detailed interaction of Ca^{2+} in the activation Ca^{2+} binding pocket for TnnC in WT complex (grey), ΔK210 complex (cyan) and ΔK210 complex in the presence of risedronate acid (purple). Specific residues coordinating the $Ca^{2+}$are shown in stick representation. **(H)** Detailed interaction of Ca^{2+} in the activation Ca^{2+} binding pocket for TnnC in ΔK210 complex in the presence of different bisphosphonate family members (Alendronate in purple, Neridronate in cyan, Ibandronate in yellow, and Pamidronate in grey). Specific residues coordinating the Ca^{2+} are shown in stick representation. Hydrogen bonds are indicated with black dashed lines.

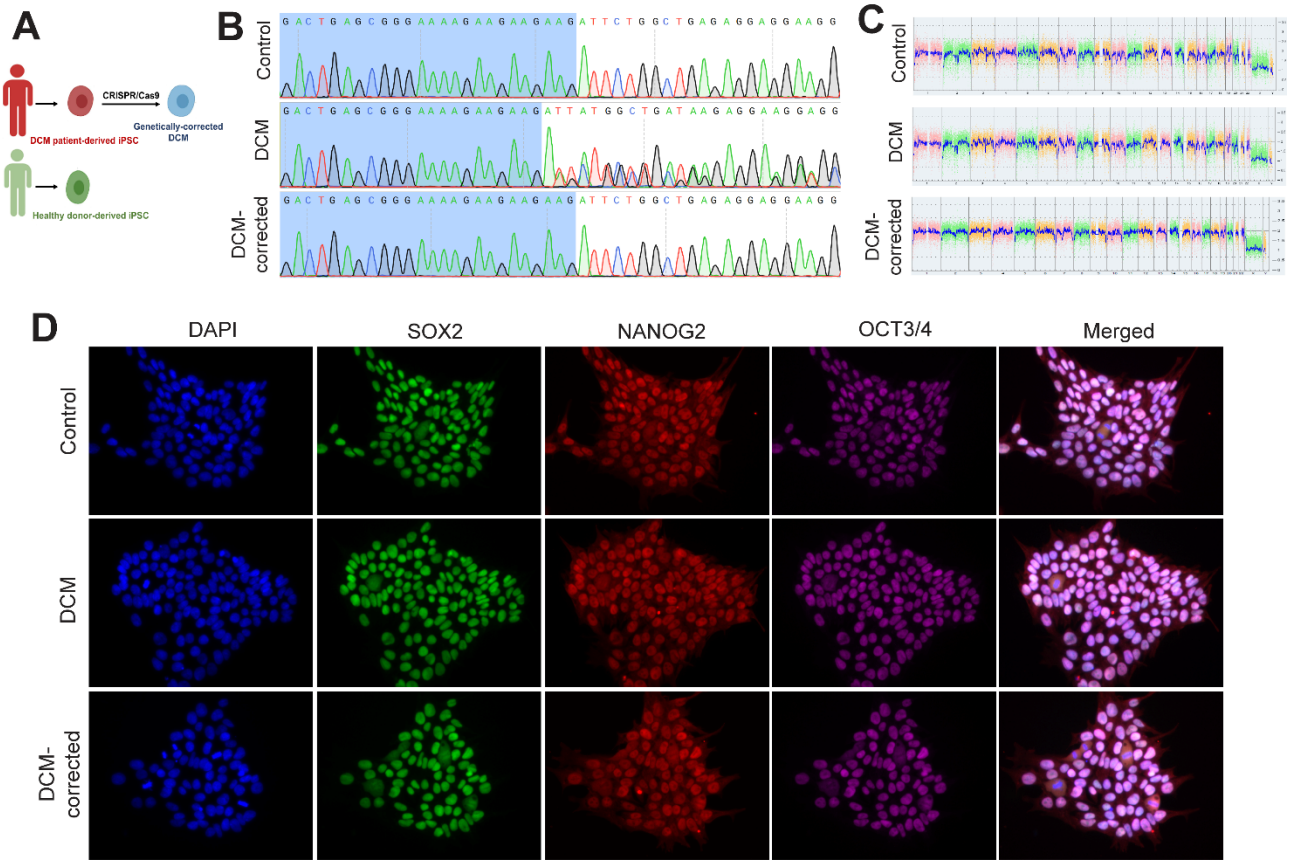

Figure S5. Generation of the heterozygous *TNNT2* K210del mutation iPSCs. (A) Schematic for isolation of iPSCs from healthy donors and DCM patients surrendered ΔK210 *TnnT* mutations. This was followed by genetically modified DCM derived iPSCs using CRISPR/Cas-9. **(B)** Sanger sequencing for WT (Ctrl), DCM, and genetically corrected DCM iPSCs. **(C)** Karyotype for WT, DCM, and genetically corrected DCM iPSCs. **(D)** Pluripotency of iPSCs WT, DCM, and genetically corrected DCM stained with DAPI (blue), SOX2 (green), NANOG (red), and OCT3/4 (purple).

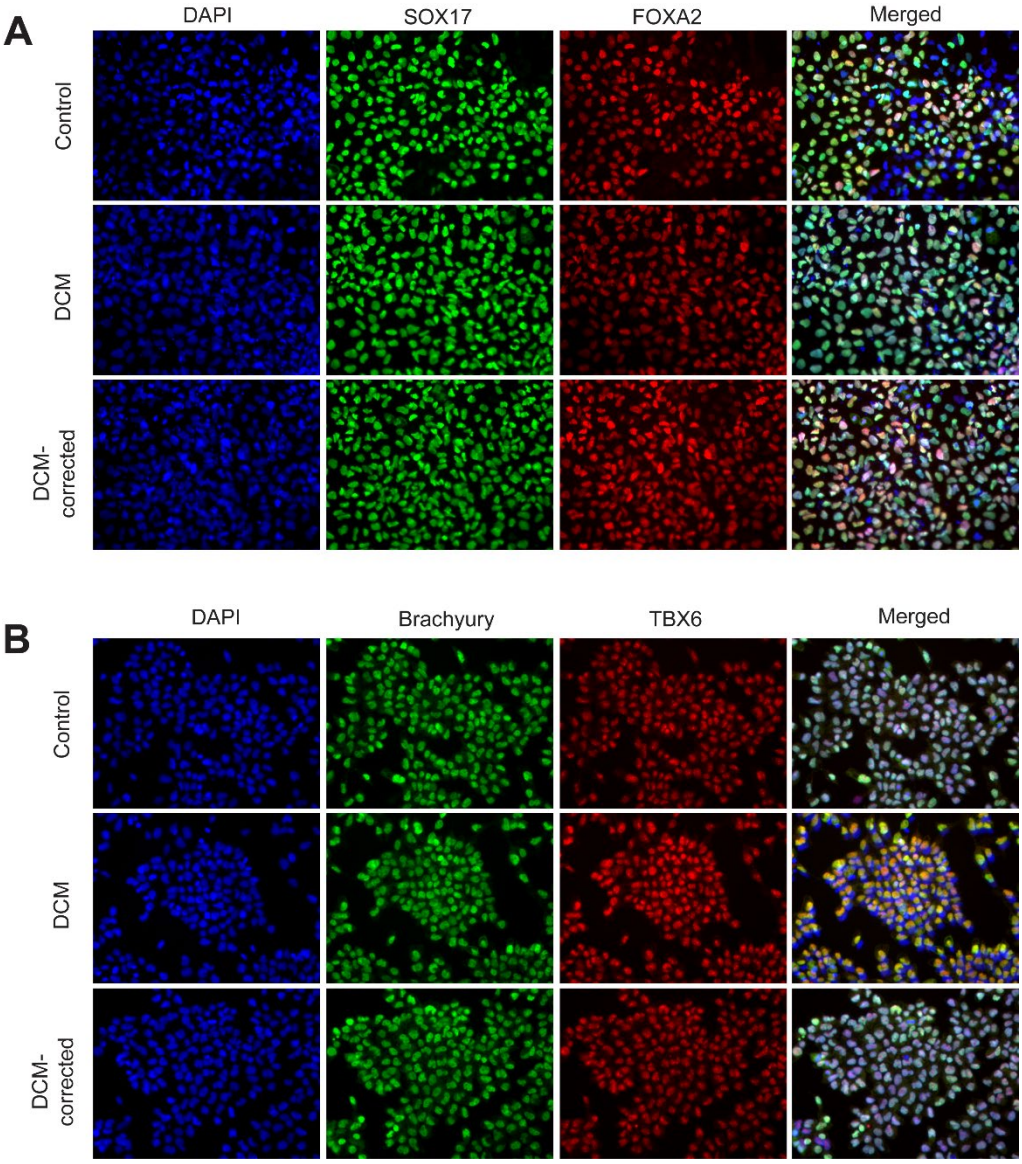

Figure S6. Confirmation of the heterozygous *TNNT2* K210del mutation iPSCs. (A) Trilineage differentiation for the endoderm of iPSCs for WT, DCM, and genetically corrected DCM stained with DAPI (blue), SOX17 (green), and FOXA2 (red). **(B)** Trilineage differentiation for the mesoderm of iPSCs for WT, DCM, and genetically corrected DCM stained with DAPI (blue), Brachyury (green), and TBX6 (red).

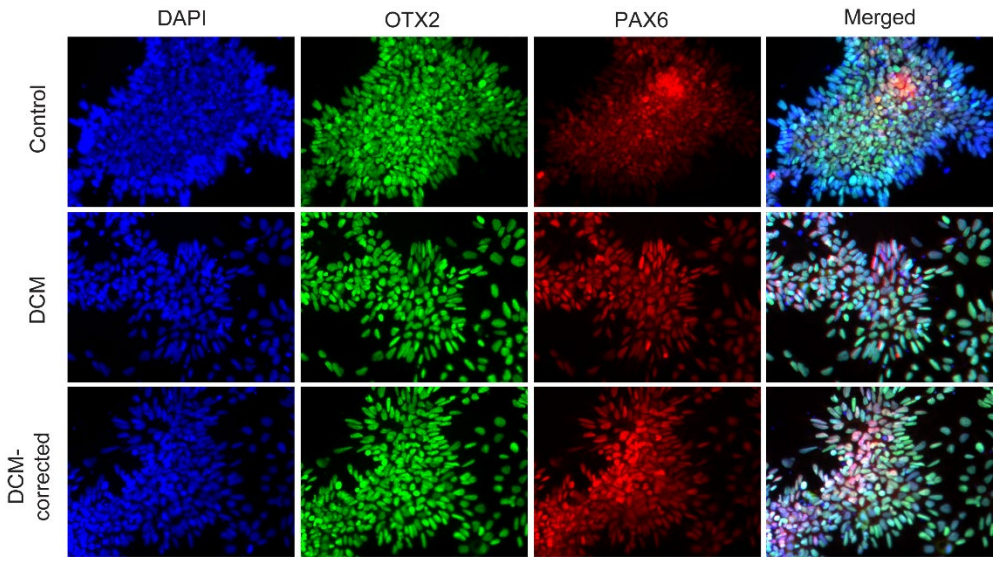

Figure S7. Confirmation of the heterozygous *TNNT2* K210del mutation iPSCs (cont.). Trilineage differentiation for the ectoderm of iPSCs for WT, DCM, and genetically corrected DCM stained with DAPI (blue), OTX2 (green), and PAX6 (red).

A

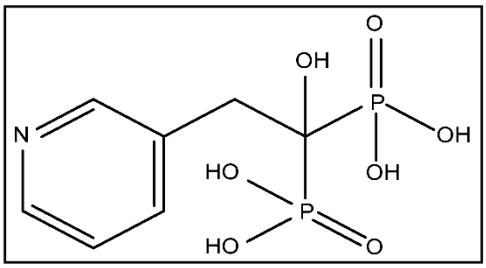

B

Non-Compartmental PK studies		
Parameter	Units	Estimate
HL_Lambda_z	min	775.3
Tmax	min	10.0
Cmax	ng/ml	213.0
AUClast	min*ng/ml	17360.80
Vz_obs	ml/kg	7919.40
Cl_obs	ml/min/kg	7.1
Vss_obs	ml/kg	4985.8

C

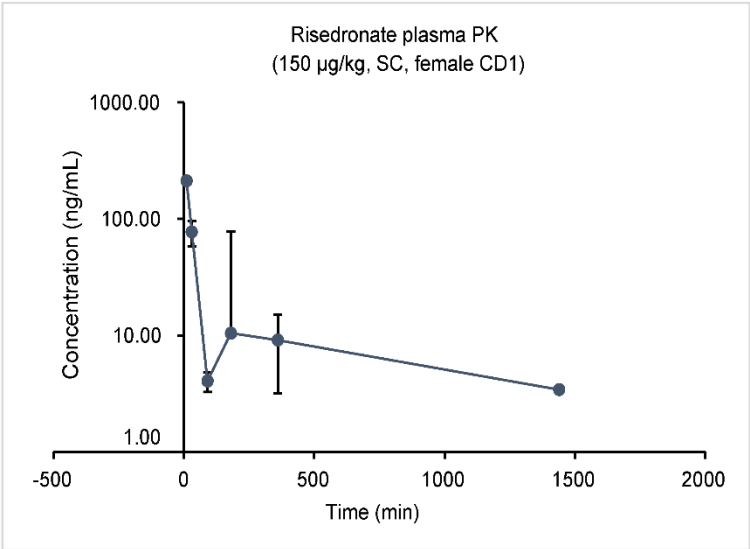

Figure S8. *In vivo* pharmacokinetic studies for subcutaneous administration of risedronate. **(A)** Chemical structure of Risedronate. **(B)** Noncompartmental pharmacokinetics parameters. **(C)** PK profiling for 150 µg/kg of subcutaneous administration of risedronate.

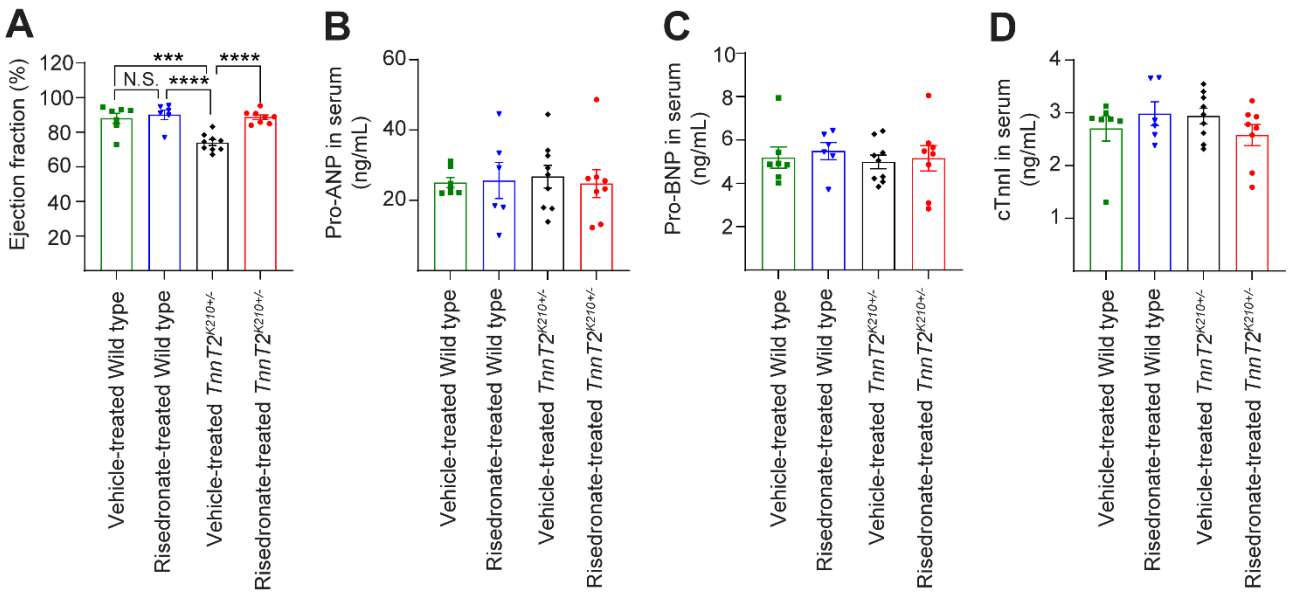

Figure S9. Risedronate treatment does not alter cardiac stress markers in *TnnT*$^{K210+/-}$ mice.

Mice were injected daily with Risedronate 150µg/kg/day, and the submandibular blood was collected 2 weeks later. **(A)** Ejection fraction. **(B)** Pro-ANP or **(C)** Pro-BNP or **(D)** TnnI was performed and analyzed using an ELISA assay. Data are mean±s.e.m. Statistical significance: one-way ANOVA with Tukey's test. *p<0.05, **p<0.01, ***p<0.001, ****p<0.001. Vehicle-treated WT, n=7; Vehicle-treated *TnnT*$^{K210+/-}$ mice, n=9; Risedronate-treated WT mice, n=6; Risedronate-treated *TnnT*$^{K210+/-}$ mice, n=8.

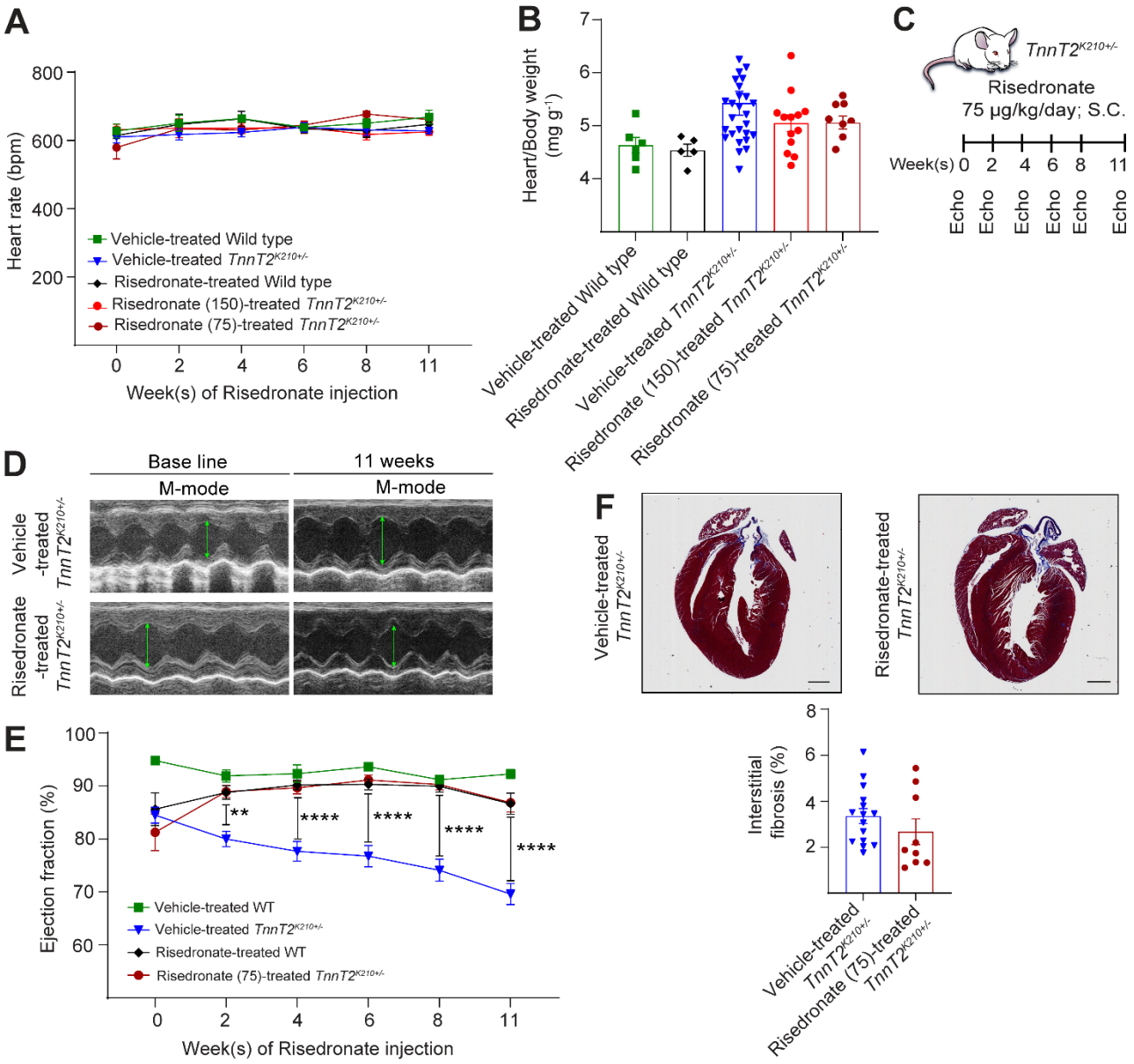

Figure S10. Risedronate treatment enhances cardiac function in *TnnT*$^{K210+/-}$ mice.

(A) Heart rate and **(B)** Heart/body weight for Vehicle- and Risedronate-treated in WT and *TnnT*$^{K210+/-}$ mice. **(C-F)** Vehicle and Risedronate administration to WT and *TnnT*$^{K210+/-}$ mice at 75µg/kg/day for 11 weeks. Schematic for treatment (C); Representative echocardiography images (D); serial echocardiography assessment of LVEF showing elevated LVEF for Risedronate-treated-*TnnT*$^{K210+/}$, compared with Vehicle-treated-*TnnT*$^{K210+/-}$mice (E), and Masson's trichrome staining of hearts, 11 weeks of Risedronate administration (75 µg/kg/day) in *TnnT*$^{K210+/-}$ mice, showing the non-significant change in the interstitial fibrosis, compared with Vehicle-treated *TnnT*$^{K210+/-}$ mice (F). Data are mean±s.e.m. Statistical significance: two-way ANOVA with Tukey's test (E). *p<0.05, **p<0.01,

***p<0.001, ****p<0.001. (A-B, E-F) Vehicle-treated-WT (n=8), Vehicle-treated-*TnnT*$^{K210+/-}$ (n=17), Risedronate-treated-WT (n=8), and Risedronate(150)-treated-*TnnT*$^{K210+/-}$(n=11), Risedronate(75)-treated-*TnnT*$^{K210+/-}$(n=9).

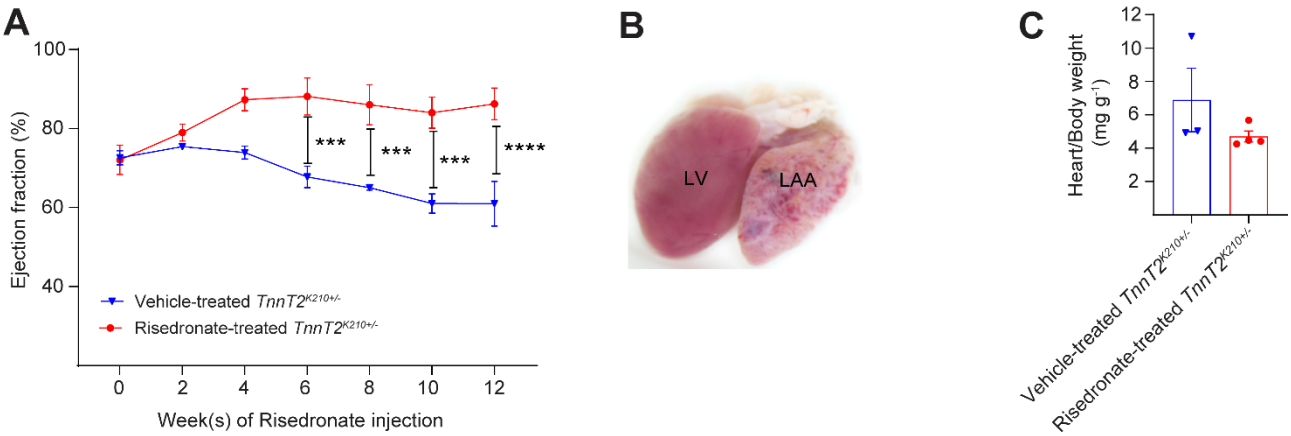

Figure S11. Risedronate treatment promotes LVEF in old *TnnT*$^{K210+/-}$ mice.

(A-C) Vehicle and Risedronate administration to one-year-old and *TnnT*$^{K210+/-}$ mice at 150μg/kg/day for 12 weeks. Serial echocardiography assessment of LVEF showing elevated LVEF on Risedronate-treated-*TnnT*$^{K210+/-}$ (A), enlarged LAA of a Vehicle-treated-*TnnT*$^{K210+/-}$ (B), and a trend of decrease in heart to body weight ratio in Risedronate-treated-*TnnT*$^{K210+/-}$, compared with Vehicle-treated-*TnnT*$^{K210+/-}$ (C). Data are mean±s.e.m. Statistical significance: two-way ANOVA with Tukey's test (A), and unpaired two-sided *t*-test (C). *p<0.05, **p<0.01, ***p<0.001, ****p<0.001. Vehicle-treated-*TnnT*$^{K210+/-}$ (n=3); Risedronate-treated-*TnnT*$^{K210+/-}$ (n=4).

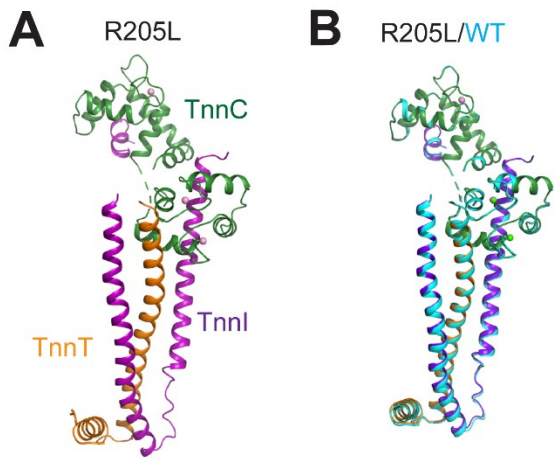

Figure S12. Structure details of R205L TnnT mutation. (A) Cartoon representation of the overall structure of the R205L complex. **(B)** Cartoon representation showing superimposition of WT (cyan) and R205L complex structures.

Ligand	WT	ΔK210	ΔK210 - risedronate	ΔK210 - pamidronate	ΔK210 - alendronate	ΔK210 - ibandronate	ΔK210 - neridronate	R205L
PDB ID	8FMM	8FMN	8FMO	8FMP	8FMQ	8FMR	8FMS	8FMT
Data collection								
Wavelength (Å)	0.9795	0.9795	0.9795	0.9795	0.9795	0.9795	0.9795	0.9795
Resolution range (Å)	50 - 3.15 (3.26-3.13)[a]	50 - 3.10 (3.21-3.10)	50 – 2.60 (2.69-2.60)	50 – 3.20 (3.31 – 3.20)	50 – 3.20 (3.31 – 3.20)	50 – 3.20 (3.31 – 3.20)	50 – 3.40 (3.52 – 3.40)	50 – 2.80 (2.90-2.80)
Space group	P 2_1	P 2_1	P 2_1	P 2_1	P 2_1	P 2_1	P 2_1	P 2_1
Unit cell (Å, °)	42.1, 168.2, 69.7 90, 101.4, 90	40.2, 170.5, 69.5 90, 101.7, 90	39.4, 169.3 69.4 90, 102.1, 90	40.2, 169.5, 70.0 90, 101.9, 90	39.5 169.7, 69.3 90, 102.1, 90	39.5 169.3, 69.4 90, 102.1, 90	40.8, 170.4, 69.7 90, 101.7, 90	42.3, 168.7, 70.1 90, 101.9, 90
Total reflections	129308	73788	169488	66531	76955	72392	58294	142936
Unique reflections	16901	15584	26261	13714	11852	13370	11980	22990
Multiplicity	7.7 (5.9)	4.7 (4.4)	6.5 (4.7)	4.9 (3.7)	6.5 (4.8)	5.4 (3.9)	4.9 (3.1)	6.2 (4.6)
Completeness (%)	99.3 (99.1)	94.2 (83.0)	98.4 (92.6)	94.5 (83.5)	85.3 (72.0)	95.9 (86.4)	97.8 (92.2)	98.4 (95.4)
Mean I/sigma (I)	12.6 (3.0)	17.7 (2.7)	20.3 (3.1)	7.8 (1.6)	10.1 (2.6)	9.1 (1.4)	10.0 (1.5)	13.7 (2.0)
CC1/2, CC*	(0.483, 0.807)	(0.903, 0.974)	(0.992, 0.998)	(0.921, 0.979)	(0.974, 0.993)	(0.970, 0.992)	(0.967, 0.992)	(0.655, 0.890)
Rmerge	0.203 (1.973)	0.076 (0.458)	0.083 (0.594)	0.213 (0.885)	0.186 (0.585)	0.173 (0.801)	0.171 (1.002)	0.129 (0.774)
Structure refinement								
R-factor/ R-free[b]	0.2296/ 0.2638	0.2387/ 0.2659	0.2148/ 0.2616	0.2599/ 0.3264	0.2834/ 0.3194	0.2613/ 0.3295	0.2553/ 0.2842	0.2416/ 0.2999
RMS (bonds)	0.003	0.002	0.005	0.002	0.002	0.002	0.002	0.003
RMS (angles)	0.647	0.486	0.922	0.552	0.448	0.532	0.450	0.620
No. of atoms	5396	5370	5427	5381	5381	5381	5381	5391
Macromolecules atoms	5390	5364	5366	5375	5375	5375	5375	5385
Ligands atoms	6	6	6	6	6	6	6	6
Water	0	0	55	0	0	0	0	0
Average B-factor	39.1	45.0	53.9	45.9	41.9	44.5	35.8	30.5
Ramachandran plot statistics								
Most favored regions (%)	93.5	93.1	96.9	89.6	94.1	90.2	93.9	92.1
Allowed regions (%)	5.7	6.1	3.1	9.6	5.3	8.9	5.5	7.6
Generously allowed regions (%)	0.8	0.8	0	0.8	0.6	0.9	0.6	0.3
Disallowed regions (%)	0	0	0	0	0	0	0	0

[a] The values for the data in the highest resolution shell are shown in parentheses.

[b] Rfree = ∑Test||Fobs| –|Fcalc||/∑Test |Fobs|, where "Test" is a test set of about 5% of the total reflections randomly chosen and set aside prior to refinement for the structure.

Table S1. Data collection and structure refinement statistics

Data collection and structure refinement statistics for troponin complexes for WT, ΔK210, ΔK210 + Risedronate, ΔK210 + pamidronate, ΔK210 + alendronate, ΔK210 + ibandronate, and ΔK210 + neridronate, and R205L.

Protein/Ligand	Ligand free	Ca^{2+}	Mg^{2+}
WT	42.8±0.5 °C	48.7±0.5 °C	46.0±0.1 °C
ΔK210	43.7±0.3 °C	50.2±0.2 °C	47.2±0.5 °C

Table S2. Melting temperature of TnnT-WT and ΔK210 at the presence and absence of different ligands.

Interacting contact between three chains after refinement

Ionic Bond

Interacting chains	Lost from WT	Newly formed in mutant K^{210del}
TnnC with TnnI	GLU126 → ARG45	ASP3 → LYS46
TnnT with TnnI		GLU213 → ARG98
TnnT with TnnC		ARG147 → ASP269

Hydrophobic interactions

Interacting chains	Lost from WT	Newly formed in mutant K^{210del}
TnnC with TnnI	PHE27 → MET154	

Hydrogen Bond

Interacting chains	Lost from WT	Newly formed in mutant K^{210del}
TnnT with TnnI	ASN271 → ARG136	

Effect of risedronate on the interacting contact between three chains after refinement

Ionic Bond

Interacting chains	Lost from WT	Newly formed in mutant K^{210del} + Rise
TnnC with TnnI		ASP3 → LYS46
TnnT with TnnI		GLU213 → ARG98
TnnT with TnnC		ARG147 → ASP269

Hydrophobic interactions

Interacting chains	Lost from WT	Newly formed in mutant K^{210del}
TnnC with TnnI		

Hydrogen Bond

Interacting chains	Lost from WT	Newly formed in mutant K^{210del}
TnnT with TnnI		

Table S3. Interacting contact between three chains after refinement for troponin complexes for WT, ΔK210, and ΔK210 + Risedronate.

Contact within the same chain after refinement

Ionic Bond

Interacting chains	Lost from WT	Newly formed in mutant K^{210del}
TnnI		LYS106 → GLU110

Hydrophobic interactions

Interacting chains	Lost from WT	Newly formed in mutant K^{210del}
TnnC	PHE20 → MET85	

Hydrogen Bond

Interacting chains	Lost from WT	Newly formed in mutant K^{210del}
TnnC	GLU94 → THR150	LYS21 → ASP25 SER35 → VAL72 ASP141 → GLY146
TnnT		GLU234 → THR238
TnnI		ARG111 → GLU115

Effect of risedronate on contact within the same chain after refinement

Ionic Bond

Interacting chains	Lost from WT	Newly formed in mutant K^{210del} + Rise
TnnI		

Hydrophobic interactions

Interacting chains	Lost from WT	Newly formed in mutant K^{210del} + Rise
TnnC		

Hydrogen Bond

Interacting chains	Lost from WT	Newly formed in mutant K^{210del}
TnnC	GLU94 → THR150	LYS21 → ASP25 SER35 → VAL72 ASP141 → GLY146
TnnT		GLU234 → THR238
TnnI		ARG111 → GLU115

Table S4. Interacting contact within the same chain after refinement for troponin complexes for WT, ΔK210, and ΔK210 + Risedronate.

	Antibody	Dilution	Company and Catalog #
Pluripotency Marker	Mouse IgG1κ Anti-SOX 2	1:200	Santa Cruz Biotechnology Cat# sc-365823
Pluripotency Marker	Mouse IgG2bκ Anti-OCT- 3/4	1:200	Santa Cruz Biotechnology Cat# sc-5279
Pluripotency Marker	Rabbit Anti-NANOG	1:200	Proteintech Cat# 142951-1-AP
Ectoderm Marker	Rabbit Anti-PAX6	1:200	Thermo Fisher Scientific Cat# 42-6600
Ectoderm Marker	Goat Anti-OTX2	1:200	R&D Systems Cat# 963273
Mesoderm Marker	Rabbit Anti-TBX6	1:200	Thermo Fisher Scientific Cat# PA5-35102
Mesoderm Marker	Goat Anti-BRACHYURY	1:200	R&D Systems Cat# 963427
Endoderm Marker	Rabbit Anti-FOXA2	1:200	Thermo Fisher Scientific Cat# 701698
Endoderm Marker	Goat Anti-SOX17	1:200	R&D Systems Cat# 963121
Secondary Antibody	Alexa Fluor 488 Goat Anti-Mouse IgG1	1:1000	Thermo Fisher Scientific Cat# A-21121
Secondary Antibody	Alexa Fluor 647 Goat Anti-Mouse IgG2b	1:250	Thermo Fisher Scientific Cat# A-21242

Secondary Antibody	Alexa Fluor 488 Donkey Anti-Goat IgG (H+L)	1:1000	Thermo Fisher Scientific Cat# A-11055
Secondary Antibody	Alexa Fluor 555 Goat Anti-Rabbit IgG (H+L)	1:500	Thermo Fisher Scientific Cat# A-21428

Table S5. Antibodies for immunocytochemistry